Received: 18 June 2021 | Accepted: 18 January 2022

DOI: 10.1111/ejn.15605

RESEARCH REPORT

EJN European Journal of Neuroscience FENS WILEY

Electrophysiological hallmarks of location-based and object-based visual multiple objects tracking

Christian Merkel[1] | **Jens-Max Hopf**[1,2] | **Mircea Ariel Schoenfeld**[1,2,3]

[1]Department of Neurology, Otto-von-Guericke University, Magdeburg, Germany

[2]Department of Behavioral Neurology, Leibniz Institute of Neurobiology, Magdeburg, Germany

[3]Kliniken Schmieder, Heidelberg, Germany

Correspondence
Christian Merkel, Department of Neurology, Otto-von-Guericke University, Leipziger Str. 44, 39120 Magdeburg, Germany.
Email: christian.merkel@med.ovgu.de

Funding information
Deutsche Forschungsgemeinschaft, Grant/Award Number: SFB1436/B05

Edited by: Ali Mazaheri

Abstract

Converging evidence shows that our visual system can track multiple visual, independently moving items over time. This is accomplished location-based by maintaining the individual spatial information of each target item or object-based by constructing an abstract object-based representation out of the tracked items. Previous work showed specific behavioural, electrophysiological and haemodynamic markers for location-based or object-based representations of the relevant targets by probing the encoded information subsequently after tracking. However, domain-specific differences of representational correlates during visual tracking itself have not been reported yet. The current study aims to identify spectral properties of the electrophysiological signal during tracking that might indicate location-based versus object-based maintenance of visual information. Subjects had to covertly track four out of eight visually identical items for several seconds while electrophysiological signals were recorded. Subsequently, a probe consisting of four items appeared and the subjects had to indicate with a button press whether the probe matched all targets or not. Subjects employing an object-based strategy showed an enhanced gamma response during the presentation of the target items at the beginning of the trial. On the other hand, subjects using a location-based strategy showed enhanced gamma synchronization throughout the tracking itself. Both the object- and location-based gamma responses yielded identical spatial topographical field distributions. These results indicate that object-based tracking is supported by enhanced encoding during the initial presentation of the targets to be tracked. Location-based tracking is characterized by the sustained maintenance of the individual targets during the entire tracking period in that same processing network.

KEYWORDS
gamma oscillations, multiple object tracking, object-based attention, principal component analysis

Abbreviations: ANOVA, analysis of variance; EEG, electroencephalography; ERF, event-related field; ERP, event-related potential; LB, location-based; MEG, magnetoencephalography; OB, object-based; PCA, principal component analysis.

1 | INTRODUCTION

The human visual system is able to keep track of several independently moving objects over the course of several seconds (Pylyshyn, 1989; Scholl et al., 2001). In typical multiple object-tracking tasks, all objects (targets and distracters) share identical visual properties, thus requiring the system to maintain each object's identity only through its unique spatio-temporal history (Kahneman et al., 1992; Pylyshyn, 2004). Classical multi-object-tracking studies modulate task difficulty by manipulating the number of relevant objects (targets) (Pylyshyn, 1989), their relative speed (Alvarez & Franconeri, 2007; Chen et al., 2013; Iordanescu et al., 2009) or their distance from one another (Alvarez & Franconeri, 2007; Franconeri et al., 2010; Shim et al., 2008). Most results suggest that, during tracking, spatio-temporal properties of the relevant objects are maintained through the individual assignment of limited spatial attentional resources (Cavanagh & Alvarez, 2005).

An alternate mechanism describes subjects to be able to allocate processing resources towards an object defined by the entire set of relevant items itself, for example, a geometrical shape constructed by illusory connections of the target objects. In a behavioural study, the conscious choice to attend all items as such one morphing object through space improved tracking ability (Yantis, 1992). In a later series of experiments, event-related electrophysiological as well as haemodynamic correlates provided converging evidence for an object-based mechanism employed to maintain multiple visual moving targets (Merkel et al., 2014, 2015, 2017). Interestingly, such a process, operating on an object-based representation derived from the configuration of all relevant targets, seems to exist in parallel with a more location-based process maintaining each individual target as described earlier (Merkel et al., 2014, 2015; Wutz et al., 2020). Furthermore, several reports suggest that the relative contribution of location-based and object-based target processing determining the individuals' performance in the tracking task can differ between subjects (Lesch et al., 2020; Merkel et al., 2014, 2015).

Neural networks involved in both tracking processes are at least partly overlapping (Merkel et al., 2015). Based on the knowledge on cognitive functions associated with the areas forming these networks, a more mechanistic description of object-based and location-based tracking is possible. A larger involvement of lateral occipital areas associated with maintaining the configurational information of the entire target set suggests a representation of a higher tier illusory object during tracking (Merkel et al., 2014, 2017). In contrast, a parametric variation of activity within parietal areas with the number of relevant targets might suggest the maintenance of single item locations through visual working memory processes (Howe et al., 2009; Jovicich et al., 2001; Merkel et al., 2014, 2015). Recent results in a patient population with lesions suggest an additional hemispheric bias for location-based and object-based tracking mechanisms (Lesch et al., 2020).

The current study aims to investigate the neurophysiological basis of the apparent location-based and object-based processes involved in maintaining multiple objects through time. For that purpose, we look at the electrophysiological spectral modulations associated with tracking. Electrophysiological oscillations specifically associated with one of the two described tracking processes provide insights of specific perceptual and cognitive processes involved during the tracking task. Especially oscillatory modulations within the gamma band are thought to indicate processes that are potentially highly relevant during location-based and object-based visual tracking like the perception of motion (Donner et al., 2007; Gruber, 1999; Hipp et al., 2011; Hoogenboom et al., 2006; Siegel et al., 2007), object-based visual processing (Adjamian et al., 2004; Kaiser et al., 2004; Kinsey et al., 2011; Rouhinen et al., 2013; Tallon-Baudry et al., 2005; Vidal et al., 2006) or visual short-term memory (Honkanen et al., 2015; Jokisch & Jensen, 2007; Lutzenberger et al., 2002; Medendorp et al., 2007; Morgan et al., 2011; Palva et al., 2011; Sauseng et al., 2009; Tallon-Baudry et al., 1998). The present work re-examines data that were previously recorded and analysed with the goal to differentiate target-related amplitude modulations between subjects favouring location-based and object-based tracking (Merkel et al., 2014).

2 | METHODS

2.1 | Subjects

Thirty-eight subjects participated in the experiment and either were paid or volunteered to gain course credit. All participants had normal or corrected-to-normal vision and were naive to the object-tracking task. The study was approved by the local ethics board and written consent was given by all subjects.

2.2 | Stimuli and task

The object-tracking task was presented on a back-projection screen at a distance of 100 cm in front of the subject placed within the dark MEG-chamber

(Vakuumschmelze). Stimuli were displayed on a black background within a field of 21° × 21° centred within the subject's field of view (Figure 1a). A white fixation cross (.5°) was present in the centre of the display throughout the experiment. At the beginning of each trial, eight identical black squares with white outline (1° × 1°) appeared randomly distributed across the field. Subsequently, four of the squares blinked every 500 ms to indicate them as relevant targets. Immediately after all eight items appeared identical again, they moved pseudorandomly within the visual field for 2800–3200 ms with a speed of 11.5°/s while the subject had to keep track of the four relevant items. The trajectories of the items were calculated offline.

The procedure for constructing the individual trajectories used was described in previous studies (Merkel et al., 2014, 2020). In short, the algorithm calculated a non-linear trajectory for each item by adding the norm vector of the sum of the current motion vector and the difference of the current position and a random virtual position to the trajectory at each frame of the motion. The virtual position changed location every 33.3–100 ms. The resulting motion appeared as a smooth non-linear path 'chasing' an imaginary jumping point. This procedure made the trajectory unpredictable and—importantly—independent of any other trajectory within the same trial. A set of eight trajectories for each trial was assembled by calculating hundreds of trajectories for each item. Then, potential trajectory permutations were combined ensuring the following constraints were met: For each frame, the minimum distance between all trajectories were above 1.8° in order to avoid occlusion, never crossed fixation and stayed within the 21° × 21° boundary. Most importantly, the calculation of the trajectories initiated with a single fixed configuration of starting points for the eight items. By subsequently reversing the motion during the experiment, it was ensured that, during each trial, the motion of all items concluded in the same final position. This is crucial, because the initial analysis of the event-related signal towards the probe appearing at the end of the motion phase could rely on a physically identical stimulus throughout all trials and conditions with otherwise pseudorandom and independent motion trajectories.

Once the motion of the items concluded, four of them appeared solid white. Those four items constituted the probe, subjects had to respond to. Not just was the spatial configuration of the eight items in this last display constant throughout all trials but also the probe within this configuration. Depending on the assignment of the

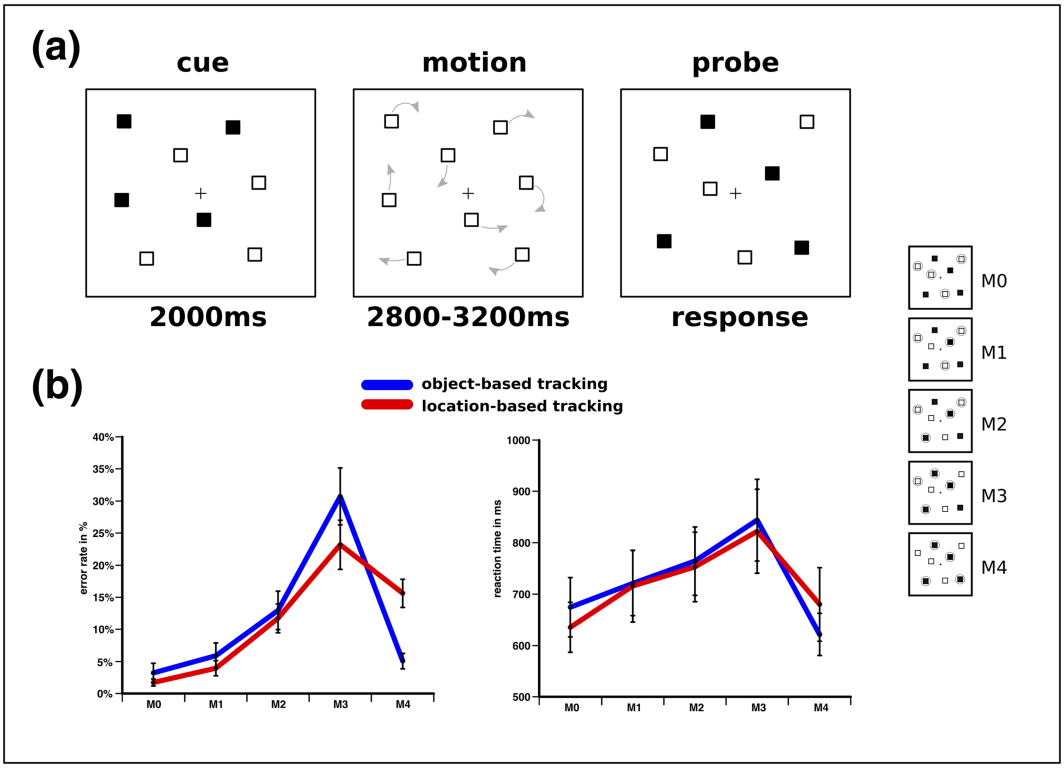

FIGURE 1 (a) Multiple object-tracking paradigm: Four out of eight items were indicated as relevant targets that subsequently had to be tracked for several seconds after which subjects had to indicate whether a probe consisting of four items was congruent with all the target items or not. (b) Subjects' responses towards the full-match condition varied considerably, indicating a different contribution of location-based and object-based tracking strategies between subjects

targets at the begin of the trial and the following trajectories, those four probes could match the relevant target items fully (M4), partly (M3, M2, M1) or not at all (M0). Subjects had to respond whether the entire probe (all four items) matched the relevant targets (M4) or not (M3–M0). After the subject's response, the next trial immediately started.

2.3 | Procedure

Subjects performed in 300 trials overall with each of the 5 experimental conditions being presented 60 times randomly distributed throughout the experiment. The experiment took approximately 45 min to complete and was divided into 10 blocks lasting 4–5 min each. Subjects were asked to fixate throughout the experiment and respond to the probe at the end of each trial as quickly and accurately as possible. Full-match responses were given with the index finger, while probes not fully matching the tracked targets had to be indicated using a button press by the middle finger.

2.4 | EEG and MEG recording

Continuous electrophysiological data were recorded while subjects performed the task using 32-channel electrodes (NeuroScan Inc., El Paso) placed according to the 10–20 system sampled with 509 Hz and an online bandpass filter of DC 200 Hz. Two electrodes placed on the left and right external canthi and one electrode below the right eye were used to record the electrooculogram. The right mastoid was used as an online reference. While setting up the electroencephalography (EEG), impedances for all electrodes were kept below 5 kOhm. The magnetencephalogram was concurrently recorded from 248 magnetometers using a BTI Magnes 2500 WH (4-D Neuroimaging, San Diego) whole head system.

For the previous analysis of the dataset (Merkel et al., 2014), the analysis of the data was carried out using BTI and ERPSS. In the current work, the raw datasets were fed into a custom pipeline using fieldtrip (Oostenveld et al., 2011), which performed all analysis steps starting from preprocessing to event-related analysis and spectral analysis. First, the EEG signal was rereferenced to the average of the right and left mastoid. EEG and magnetoencephalography (MEG) data were subsequently low-pass filtered at 254 Hz. The continuous datasets were then epoched from −2000 to 2500 ms time-locked to the onsets of the cue, the onset of the motion of the items and the onset of the probe, resulting in 900 EEG and MEG epochs each. For the EEG dataset, an additional artefact reduction step was introduced using an independent component analysis. Individual components within the EEG datasets representing likely ocular artefacts based on their scalp topography were automatically detected and removed (Drisdelle et al., 2017; Li et al., 2006). We performed additional analyses (shown in the supporting information) to ensure that there were no task-specific differences in the gamma band due to eye movements. The decision of removing particular components was based on the topographical distribution of their local signal gradients by averaging the derivatives of all surrounding electrodes relative to each electrode. Components were rejected if this spatial derivative of its topography was larger by a factor of 2.5 across frontal electrodes (VEOG, HEOG, Fp1, Fp2, F8, F4, Fz, F3, F7, T8, C4, FC2, FC1, C3, T7) compared with the remaining central and posterior electrodes. During the current analysis, four subjects were removed due to excessive high-frequency noise. All subsequent analyses are based on 34 instead of 38 subjects included for the previous report.

For the following event-related analysis, EEG and MEG epochs, time-locked to the probe, underwent additionally a separate artefact rejection step employing an individual and flexible peak-to-peak criterion, removing 15% of trials with the largest amplitude differences within each subject. Subsequently, event-related potentials (ERPs) and event-related fields (ERFs) were baseline corrected (−200 to 0 ms relative to probe onset) and averaged, time-locked to the onset of the probe, separately for the five match conditions.

For calculating the spectral power modulation of the EEG and MEG signals across the time course of each trial, epochs, time-locked to the motion onset, of trials that subjects responded correctly to, were utilized. Thus, changes in spectral power during successful target maintenance relative to the cueing phase could be observed. For those sets of epochs, the same individual artefact rejection criterion (peak-to-peak, 15%) was employed. Subsequently, induced time-frequency modulations were calculated for all EEG and MEG channels for each trial during a time window of −1500 to 2000 ms relative to motion onset using a sliding Hanning window of 200 ms in 20-ms steps from 5 to 120 Hz. Time-frequency data were baseline-corrected (−200 to 0 ms relative to motion onset) and averaged across all included trials.

2.5 | Data analysis

2.5.1 | Behaviour

Differences in reaction time and accuracy across match conditions were investigated using a repeated measures

analysis of variance (ANOVA) with a five-level factor (M0/M1/M2/M3/M4). Based on the behavioural variance between subjects, particularly during the full-match condition, a median split was performed, dividing the subjects into two performance groups. The differences in accuracy between the M4 and M0 conditions were used for that purpose. Subjects exhibiting equal or higher accuracies for full-match trials compared with zero-match trials were considered 'object-based' trackers. Subjects performing considerably worse during fully congruent trials compared with trials in which no probe matched the prior target set were considered 'location-based' trackers. As previously reported, subjects vary in their representational bias during tracking showing either a location-based (LB) or object-based (OB) tracking preference. The allocation into two different performance groups based on performance was maintained as between-subject factor throughout the analysis.

2.5.2 | Event-related analysis

ERPs as well as event-related magnetic fields were analysed time-locked to the onset of the probe. The probe display evoked two classical visual components (N1/N2) that peaked around 180 and 280 ms, respectively, across all conditions. Mean amplitudes for these two components within two different time windows, 170–210 and 270–310 ms, were compared between match conditions (M0/M1/M2/M3/M4) as a five-level within-subject factor and between performance groups (LB/OB) as a two-level between-subject factor using a two-factorial mixed model design. The amplitudes for the ERPs were averaged across occipital electrodes (O9, Iz, O10) where modulations by the visual probe were maximal. Likewise, ERFs were averaged across neighbouring posterior sensors (A139, A140, A141, A168).

2.5.3 | Time-frequency analyses

Induced event-related changes in signal power were calculated for all electrodes and sensors for the tracking period relative to motion onset. Thus, a frequency power representation for a 1.5-s cueing period as well as a concluding 2-s motion phase for a frequency range from 5 to 120 Hz could be analysed. First, the signal within three frequency bands showing considerable modulation in both modalities (EEG/MEG) was averaged resulting in three power modulations over time for signals in the alpha and beta range (8–30 Hz), low-gamma range (50–80 Hz) and high-gamma range (80–110 Hz). In order to reduce the dimensionality of each of those three signals within each of the two modalities (EEG/MEG) and extract shared temporal morphologies across electrodes or sensors, principal component analyses (PCAs) were performed for each of the three frequency modulations within each modality on the data averaged across all subjects. This approach resulted in spatial load distributions for the EEG and MEG modality for each component and the corresponding temporal morphology shared across all subjects. In order to investigate differences in those time courses across groups, the resulting unmixing-matrices for each PCA (one for each frequency band and modality) were subsequently multiplied with the power modulation across time of each single subject to calculate the individual contribution of each subject's signal to each component of the averaged signal. This approach allowed for statistical comparisons between the temporal morphologies of the two performance groups as it circumvents the multiple comparison problem posed by testing power modulations within an electrode/sensor × time × frequency × group space. In the current case, the group difference of only a single temporal morphology of a relevant component has to be considered. Each time courses of the components were additionally averaged across the cueing and motion phase for each subject. Two-factorial repeated measures analysis of variance (rANOVA) were applied to test for differences in power modulations across time (cue/motion) as a within-subject factor and between groups (OB/LB) for certain components in different frequency bands within the two modalities. In order to account for potential deviation of variance homogeneity between performance groups after the median split, between-group effects were additionally tested using permutation tests with 1000 randomizations of group assignments. For group comparisons, the corrected *p*-values based on these distributions derived from the permutation tests are reported with the standard *p*-values. Tests were performed for components within the frequency bands and modalities, with topographical distributions of the factor loads clearly indicating sensory and cognitive sources.

3 | RESULTS

3.1 | Behaviour

Behavioural performances in the tracking task were examined excluding four subjects (two per performance group). Error rates and reaction times differed across match conditions ($F_{4,\ 128} = 56.588$, $p < .001$, $e = .639$/$F_{4,\ 128} = 27.583$, $p < .001$, $e = .463$). Reactions towards the full-match probe deviated from an otherwise linear decrease in performance with an increase in probe match

(Figure 1b). Responses for a full match were more accurate ($t_{33} = 5.164$, $p < .001$, $e = .447$) and faster ($t_{33} = 5.849$, $p < .001$, $e = .509$) compared with responses for the match-3 condition. Additionally, error rates for the match conditions differ between the performance groups ($F_{4, 128} = 6.778$, $p = .005$, $e = .175$). This effect is mostly driven by a lower accuracy during the full-match condition in the LB group compared with the OB group ($t_{32} = 4.213$, $p < .001$, $e = .357$). Error rates were also lower for the full-match condition compared with the match-3 condition within the OB group ($t_{16} = 6.361$, $p < .001$, $e = .717$) but not for the LB group ($t_{16} = 1.88$, $p = .078$, $e = .181$). Overall accuracy was not different between groups ($F_{1, 32} = .15$, $p = .902$, $e < .001$).

3.2 | Event-related results

The EEG signal elicited by the various match probes shows a different time course for the two performance groups. The mean amplitudes during 170–210 ms neither show a main effect for match conditions ($F_{4, 128} = .677$, $p = .59$, $e = .021$) nor for group ($F_{1, 32} = 1.059$, $p = .31$, $e = .032$) in a two-factorial rANOVA (Figure 2a). However, the variation of the mean amplitudes within this time window across the match conditions is different between the performance groups ($F_{4, 128} = 3.111$, $p = .023$, $e = .089$), with amplitudes within the OB group showing a significant effect of match condition ($F_{4, 64} = 2.772$, $p = .05$, $e = .148$) while amplitudes within the LB group were not different between match conditions ($F_{4, 64} = 1.034$, $p = .38$, $e = .061$). The match effect within the OB group is driven by a higher amplitude for the full-match condition compared with the match-3 condition ($t_{16} = 2.424$, $p = .028$, $e = .269$). Moreover, the amplitude for the full match during the 170- to 210-ms time window is higher in the OB group compared with the LB performance group ($t_{32} = 2.227$, $p = .033$, $e = .134$).

The mean EEG amplitudes during the 270- to 310-ms time windows show a gradual decrease with increasing match for both performance groups ($F_{4, 128} = 17.529$, $p = .001$, $e = .354$/G1: $F_{4, 64} = 5.671$, $p = .008$, $e = .262$/G2: $F_{4, 64} = 13.391$, $p = .001$, $e = .456$). The amplitudes within 270–310 ms were not different between groups ($F_{1, 32} = 1.78$, $p = .192$, $e = .053$). The amplitude decrease with condition did not exhibit any significant difference ($F_{4, 128} = .359$, $p = .749$, $e = .011$). These results are virtual identical with those reported earlier (Merkel

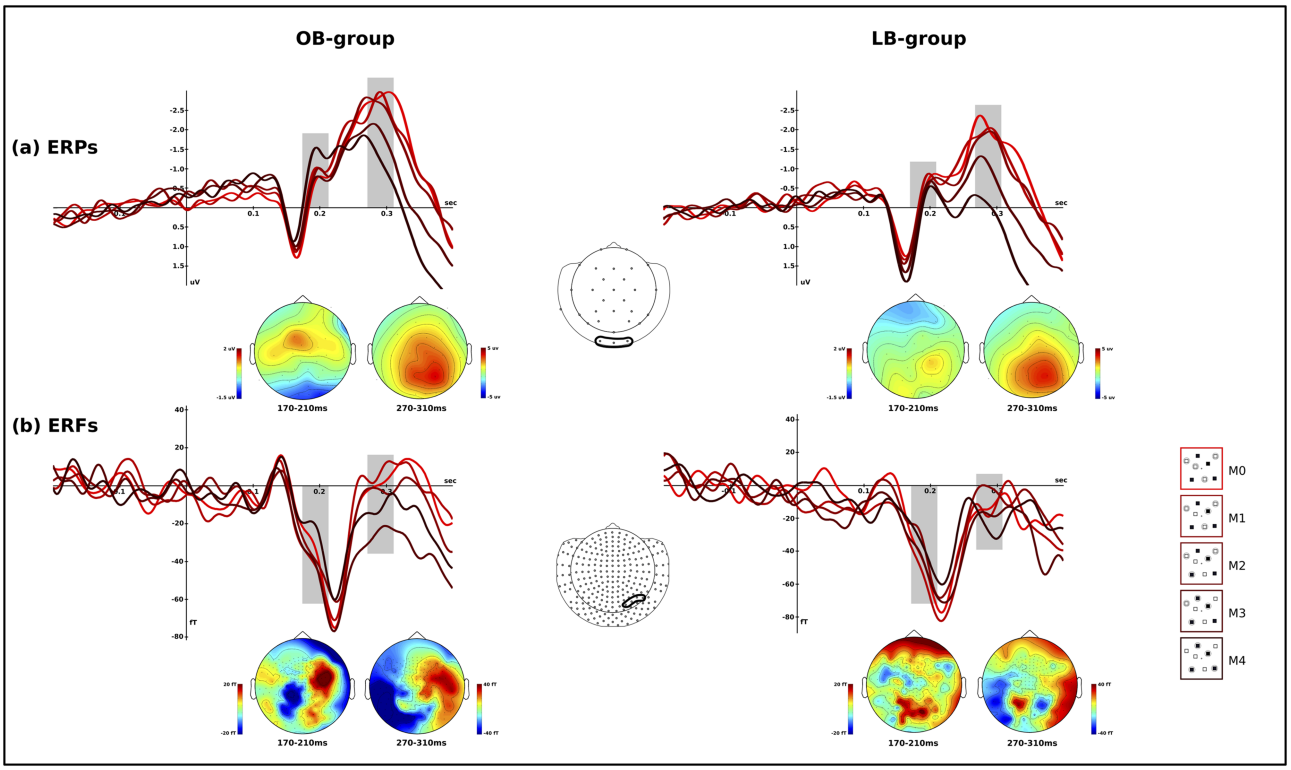

FIGURE 2 Event-related electrophysiological responses time-locked to the onset of the probe. Both subject groups, showing location-based as well as object-based tracking, show a parametric response between 270- and 310-ms response that varies in amplitude with target-probe congruity for EEG (a) and MEG (b) modalities. Additionally, an earlier amplitude enhancement (170–210 ms) is elicited exclusively by the full-match condition in the object-based tracking group only

et al., 2014) on the same dataset but excluding four subjects and using a different analysis pipeline.

Figure 2b displays the amplitude modulations for the ERF signal across probe conditions for the two performance groups. Although the coarse morphology is similar to the ERP modulations, especially ERFs within the LB group contain far more noise. Amplitudes during the 170- to 210-ms time range neither showed a significant effect of match condition ($F_{4, 128} = 2.052$, $p = .106$, $e = .06$), performance group ($F_{1, 32} = .261$, $p = .613$, $e = .008$) nor any interaction ($F_{4, 128} = .575$, $p = .646$, $e = .018$). The full-match condition however showed a trend for a higher amplitude compared with the match-3 condition for the OB group ($t_{16} = 2.09$, $p = .062$, $e = .201$), but not for the LB group ($t_{16} = 1.147$, $p = .268$, $e = .076$). During the 270- to 310-ms time range, ERFs differed between match conditions ($F_{4, 128} = 2.743$, $p = .041$, $e = .079$) in a linear fashion ($F_{4, 32} = 4.148$, $p = .05$, $e = .115$). These amplitude changes across match conditions were not different between performance groups ($F_{4, 128} = 1.092$, $p = .359$, $e = .033$).

3.3 | Time-frequency results

Figure 3 illustrates the relative power changes of the electroencephalographic and magnetoencephalographic signals across a spectrum of 5–120 Hz within the channels (O9/Iz/O10) and sensors (A139, A140, A141, A168) used for the event-related analysis of the probe-related signal throughout the cueing and tracking phase of all correct trials. The data are separately shown for the object-based tracking group (Figure 3a) and the location-based tracking group (Figure 3b). First, a striking low-frequency desynchronization with the onset of the movement between 8 and 30 Hz can be observed across performance groups (OB/LB) and modalities (EEG/MEG). Over a broadband gamma range, a general increase in signal power can be observed during tracking within the MEG signal. A strong interaction for the amplitude of the broadband gamma signal (>50 Hz) between the timing (cueing/motion phase) and the performance groups (OB/LB) was observed in the EEG.

In order to detect the underlying sources of these effects, distinguish their common spatial topography amongst all subjects from spurious, unrelated power changes, and quantify their unique temporal morphologies, time courses of three separate frequency bands were averaged across all subjects and entered into individual PCAs for each of the frequencies and modalities. Amplitude modulations of relevant components for each frequency range and modality (EEG/MEG) were entered into a two-factorial rANOVA with the factors time (cue/motion) and performance group (OB/LB).

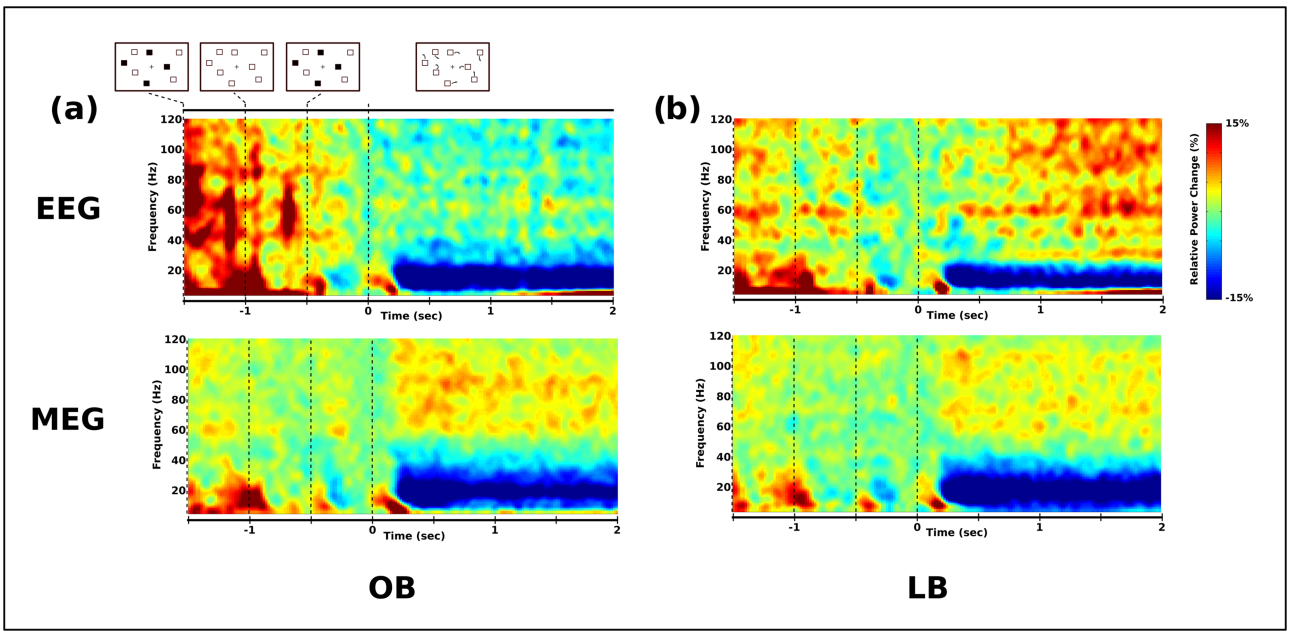

FIGURE 3 Time-frequency plots for both modalities averaged over electrodes O1, Oz, O2 for EEG and sensors A139, A140, A141, A168 for MEG. The spectral power changes over the time course of the cueing and movement phase relative to a 200-ms window shortly before the onset of the tracking are illustrated for both object-based (a) and location-based (b) groups separately. The EEG modality shows a clear difference in broadband gamma amplitude during cue presentation and attentive tracking between performance groups. (a) Amplitude changes in the gamma range seem to be induced by the stimulus transient of the cue in the object-based tracking group. (b) During the motion phase in the location-based tracking group, a clear elevation of synchronization within the gamma range can be observed

The first principal component for the alpha/beta frequency range captured the low-frequency desynchronization with the onset of the motion within the EEG model ($F_{1, 32} = 109.541$, $p < .001$, $e = .774$) as well as the MEG model ($F_{1, 32} = 49.363$, $p < .001$, $e = .607$). This alpha/beta desynchronization component exhibited a broad posterior distribution within both modalities (Figure 4a). The low-frequency power neither was different between performance groups (EEG: $F_{1, 32} = 1.128$, $p = .296$ [$p_{perm} = .311$], $e = .034$; MEG: $F_{1, 32} = .328$, $p = .571$ [$p_{perm} = .251$], $e = .01$) nor showed an interaction over time (EEG: $F_{1, 32} = 1.903$, $p = .177$ [$p_{perm} = .184$], $e = .056$; MEG: $F_{1, 32} = .023$, $p = .882$ [$p_{perm} = .251$], $e = .001$).

The differences of the low-gamma power modulation (50–80 Hz) over time between the performance groups for the EEG became apparent within the second principal component of the model ($F_{1, 32} = 6.529$, $p = .016$ [$p_{perm} = .005$], $e = .169$) (Figure 4b). The gamma amplitude not just increased within the LB group during motion relative to the cue period ($t_{16} = 3.0$, $p = .008$, $e = .36$) but was also increased during tracking compared with the OB group ($t_{32} = 2.564$, $p = .015$ [$p_{perm} = .006$], $e = .17$). Interestingly, peaks of gamma amplitude enhancements were apparent, time-locked to visual cue transients solely within the OB group. This components' topography showed a bilateral occipital distribution. Within the MEG modality, an equivalent significant interaction effect was not observed ($F_{1, 32} = .441$, $p = .511$ [$p_{perm} = .218$], $e = .014$), although, during motion, the LB group exhibited a larger amplitude enhancement for the 50- to 80-Hz range compared with the OB group ($t_{32} = 2.068$, $p = .047$ [$p_{perm} = .023$], $e = .118$). Furthermore, the low-gamma signal exhibited

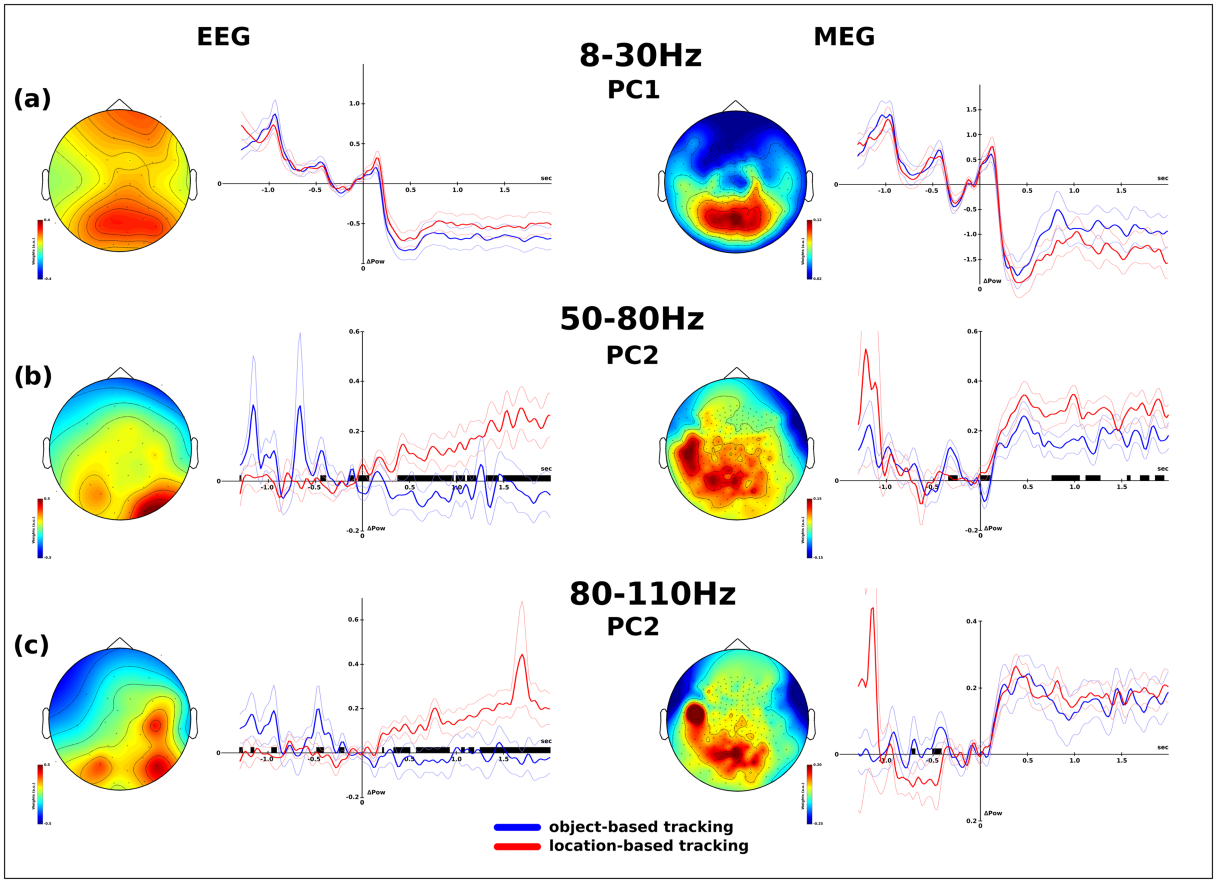

FIGURE 4 Principal component analysis for three frequency ranges of interest, separately for the EEG and MEG modality. PCAs were performed on the average signal of all subjects. Subsequently, each individuals' projection onto the calculated components were derived using the unmixing matrix of the initial PCA. The temporal morphologies of each component were thus compared between the two performance groups. Mean morphology (bold line) and standard deviation (thin lines) are illustrated for both groups in each component. (a) The frequency range of 8–30 Hz shows a strong desynchronization with onset of the motion in both performance groups. This effect loads heavily on central posterior electrodes and sensors. (b,c) Within the gamma range (50–80 Hz (b) and 80–110 Hz (c)), components with a mostly bilateral occipital distribution in the EEG modality and corresponding sources in the MEG modality show a different temporal morphology between performance groups with higher synchronization of the location-based group during tracking and higher synchronization of the object-based group during cueing

a general power increase during the motion phase compared with the cueing phase ($F_{1, 32} = 8.328$, $p = .007$, $e = .207$). This components' more posterior distribution was roughly consistent with the EEGs topography.

The analyses for the amplitude modulations within the high-gamma range of 80–110 Hz revealed similar results to the range between 50 and 80 Hz for the EEG modality (Figure 4c). The second component of that model showed the same bilateral occipital distribution and its morphology showed a similar interaction between time period and performance group ($F_{1, 32} = 8.073$, $p = .008$ [$p_{perm} = .004$], $e = .201$). The 80- to 110-Hz signal increased during tracking within the LB group ($t_{16} = 3.038$, $p = .008$, $e = .366$) and was higher compared with the OB group ($t_{32} = 2.515$, $p = .017$ [$p_{perm} = .006$], $e = .165$). Interestingly, although not significant across the whole cueing period ($t_{16} = 1.259$, $p = .226$, $e = .9$), the OB group exhibited the same amplitude peaks related to cue transients as observed within the low-gamma signal. These were slightly elevated compared with the LB group according to the permutation statistic ($t_{32} = 1.650$, $p = .109$ [$p_{perm} = .048$], $e = .078$).

The MEG component capturing the modulation of the signal within the 80- to 110-Hz range exhibited a similar topography as within the 50- to 80-Hz range. However, the higher signal during the motion phase ($F_{1, 32} = 9.043$, $p = .005$, $e = .22$) was not different between performance groups ($t_{32} = .266$, $p = .792$ [$p_{perm} = .429$], $e = .002$) anymore.

One main objective of the principal component decomposition was to distinguish temporal morphologies of cognitive sources from spurious effects of micro saccades within the gamma signal. For both analysed gamma ranges, the respective primary component hereby successfully captured ocular sources within the EEG and MEG modality (Figure 5). Those components showed a higher amplitude during the cue compared with the tracking phase in both gamma ranges and both modalities (EEG [50–80 Hz]: $F_{1, 32} = 13.568$, $p < .001$, $e = .298$; MEG [50–80 Hz]: $F_{1, 32} = 13.235$, $p < .001$, $e = .293$, Figure 5a; EEG [80–110 Hz]: $F_{1, 32} = 7.966$, $p = .008$, $e = .199$; MEG [80–110 Hz]: $F_{1, 32} = 9.367$, $p = .004$, $e = .226$, Figure 5b). It is furthermore noteworthy that although the electroencephalographic distribution biased towards ocular sources tended to be elevated for the LB group compared with the OB group ([50–80 Hz]: $t_{32} = 1.537$, $p = .134$, $e = .069$; [80–110 Hz]: $t_{32} = 1.697$, $p = .099$, $e = .083$), the corresponding occipital factor loads exhibit the opposite sign compared with those of the cognitive sources observed within the second component. This indicates that the component analysis is able to reliably separate cognitive from microsaccadic amplitude variations.

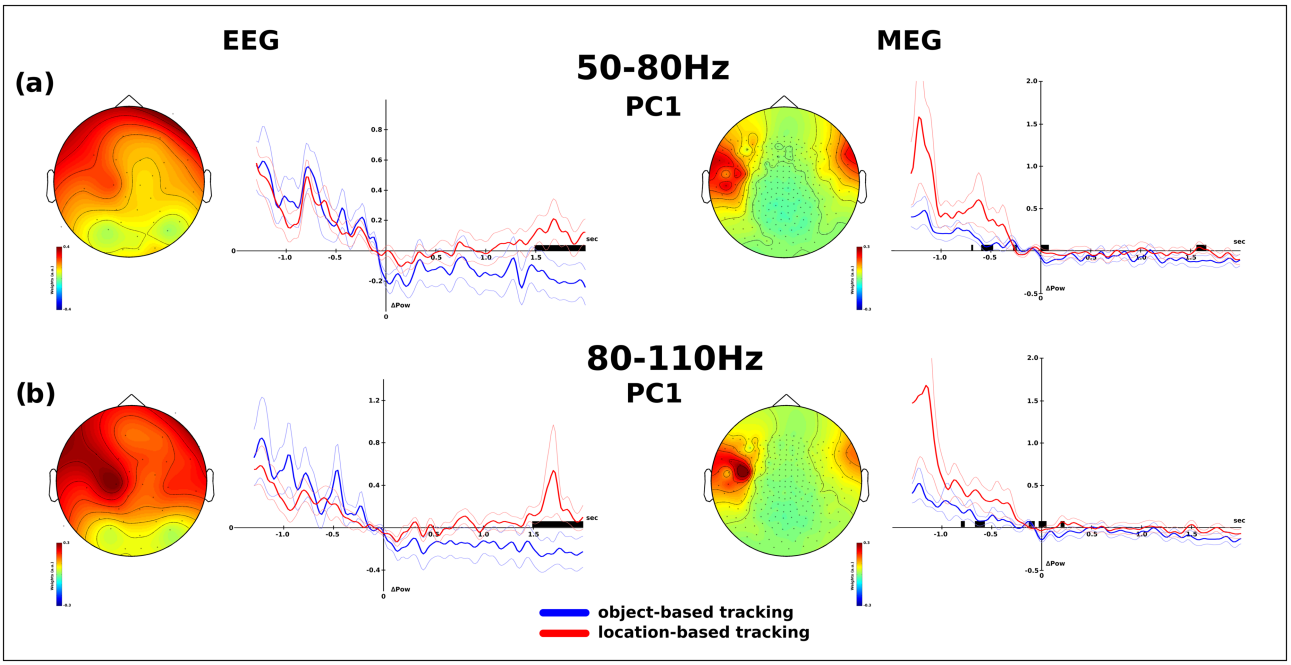

FIGURE 5 Primary principal components for the gamma frequency ranges capturing ocular sources. The first components for the low- (a) and high- (b) gamma PCA analyses show spatial distributions consistent with microsaccadic activity. The temporal morphologies of those ocular components suggest a higher rate of occurrence in micro saccades during the cueing phase. Importantly, those ocular morphologies do not explain the gamma variation between performance groups

4 | DISCUSSION

The current data revealed behavioural inter-subject differences in strategy employment in order to maintain multiple moving objects over the course of several seconds. In line with previous work, these behavioural differences correlated with an early event-related component elicited by probed targets presented at the end of the tracking period to which subjects had to respond (Merkel et al., 2014). The current work provides evidence that these behavioural differences, associated with object-based and location-based information maintenance, are also associated with earlier systematic differences of oscillatory activity within a broad gamma frequency range, namely, during the tracking itself.

Insights of electrophysiological spectral modulations during multiple object tracking are sparse and not entirely conclusive. While a general desynchronization within the alpha range together with a load-dependent increase in gamma activity during tracking (Rouhinen et al., 2013) were observed before, recent work found an increase in alpha power during object tracking for both location-based and object-based tracking tasks (Wutz et al., 2020). The observed desynchronization of induced oscillations within the low-frequency range during the present study is in line with the nature of object tracking as an attentional demanding task (Kinsey et al., 2011; Worden et al., 2000). The acquisition of additional attentional resources during tracking is suggested to be accompanied by the disinhibition of occipital and parietal areas indicated by a desynchronization of alpha oscillations (Klimesch et al., 2007; Pfurtscheller, 2001). Importantly, one important aspect of the object-tracking task is the update and maintenance of visual information during the tracking involving working memory mechanisms (Alvarez & Franconeri, 2007; Drew & Vogel, 2008). The modulations observed for oscillatory signals in the alpha range during the delay period of working memory tasks are multifaceted and highly dependent on the spatial or non-spatial nature of the task (Kelly et al., 2006; Medendorp et al., 2007). Increases in alpha power during the retention period were load dependent and could be observed in experiments using Sternberg's paradigms or in other non-spatial delayed-match-to-sample tasks (Busch & Herrmann, 2003; Jensen et al., 2002; Sauseng et al., 2005). On the other hand, a number of studies suggest an inverse relationship between the representational load or demand during a memory delay and alpha synchronization (Gevins et al., 1997; Krause et al., 2000; Okada & Salenius, 1998; Pesonen et al., 2007), stressing instead the involvement of attentional control mechanisms during visual working memory tasks (Palva et al., 2011; Sauseng et al., 2009; Singh et al., 2002). The current dataset is well in line with this later interpretation of low-frequency desynchronizations as an indicator of an enhanced involvement of processing resources during visual tasks. A decrease of alpha and beta power can be observed over central parietal regions as the tracking period starts. This desynchronization was not different for object-based versus location-based tracking strategies, suggesting a more general rather than specific mechanism of enhanced visual cognitive engagement. Similarly, modulations of beta power during visual tasks have been linked to mechanisms exerting a different degree of top-down versus bottom-up control over visual perception (Bastos et al., 2015; Buschman & Miller, 2007; Michalareas et al., 2016; Richter et al., 2017). Hereby, increased beta synchronization was suggested to reflect resilience of the perceptual states against external stimulation (Belitski et al., 2008). These internal perceptual states might well be altered by endogenous processes (Battaglini et al., 2020; Okazaki et al., 2008; Ronconi et al., 2016; von Stein et al., 2000). In the same vein, stimulus-driven perceptual transitions are in contrast related to a decrease in beta oscillations (McCusker et al., 2020; Zaretskaya & Bartels, 2015). Such transitions are forced in the current task by presenting unpredictable motion stimuli, requiring the visual system to be receptive to a continuously changing visual input.

In general, low-frequency desynchronizations (alpha and beta) also have consistently been observed with the onset of moving stimuli (Donner et al., 2007; Hipp et al., 2011; Siegel et al., 2007), which further adds to the general effect of power decrease in the frequency range between 8 and 30 Hz for both performance groups. In sum, the observed low-frequency desynchronization in our data seems to represent a general involvement of cognitive resources at least in part driven by the bottom-up processing of the stimuli relevant to the task.

The decrease of low-frequency power is frequently reported to be accompanied by a consistent and synchronous increase across a broad gamma range in visual tasks with moving stimuli (Donner et al., 2007; Hipp et al., 2011; Hoogenboom et al., 2006; Siegel et al., 2007) but also in tasks requiring the retention of visual information in working memory (Jokisch & Jensen, 2007; Medendorp et al., 2007; Morgan et al., 2011). The sustained synchronization of the gamma signal during the active maintenance of visual representations is hereby thought to increase with the demands of the task (Kaiser et al., 2003; Morgan et al., 2011; Tallon-Baudry et al., 1998) or with the working memory load (Honkanen et al., 2015; Jokisch & Jensen, 2007; Palva et al., 2011). Consistent with these findings, the current data show a sustained increase of gamma signal with bilateral occipital field topographies for subjects

employing a location-based tracking strategy. With respect to the working memory load, the representation/retention of the information based on the four separate individual locations is known to require the involvement of processing resources close to the cognitive limit (Cowan, 2001). The current data are well in line with the idea of a resource challenging working memory process.

Although the temporal morphology of the gamma modulation is mostly similar for the EEG and MEG modalities, for the high-frequency gamma range in the magnetoencephalographic signal, performance groups do not significantly differ in their gamma enhancement during the tracking phase. Gamma modulations are a result of local excitatory network communications (Kopell et al., 2000) and induce therefore a more localized signal within a more narrow frequency band within the MEG compared with the EEG signal (Kaiser et al., 2003; Lutzenberger et al., 2002; Tallon-Baudry et al., 1997). Observed modality differences in effect sizes could well be explained, whereas the overall between- and within-subject effects remain similar.

Interestingly, subjects employing an object-based tracking strategy do not show any modulation in gamma power in the EEG nor the MEG signal with the onset of the tracking phase in the current task.

The integration of individual features during delayed-match-to-sample tasks have been associated in previous studies with a relative increase in gamma signal during the retention interval (Honkanen et al., 2015; Morgan et al., 2011; Vidal et al., 2006). Likewise, other object-based processes like figure-ground segmentation (Kinsey et al., 2011) or the perception of illusory objects (Kaiser et al., 2004; Tallon-Baudry et al., 1997) have been described to induce enhanced gamma activity. We have previously suggested the maintenance of an abstract (illusory) object representation in the lateral occipital to be the key process involved in the object-based tracking strategy (Merkel et al., 2015, 2017), and therefore, we would have expected gamma modulations related to object-based processes. The absence of gamma signal modulations during the tracking phase in the current results is a bit surprising and seemingly at odds with previous findings relating gamma modulations to object processing. However, while absent during the tracking phase, short enhancements time-locked to the visual cue transients (onsets, offsets) prior to the tracking phase are present in the EEG data exclusively for the object-based performance group. This would suggest an enhanced encoding of the object information within the object-based performance group compared with the location-based performance group during the cue phase prior to motion onset, which would be well in line with the previously mentioned work. Enhanced transient gamma responses in the high-frequency band towards visual objects are evoked by enhanced visual attention processes (Fries, 2001; Tallon-Baudry et al., 2005) and thus indicate improved encoding. The encoding of the relevant information during the cueing phase of the tracking task builds up a central representation setting the stage for the subsequent maintenance during the tracking period. The tracking itself just requiring updating of special information does not seem to have a specific time-frequency fingerprint in the current experiment.

Importantly, the enhanced transient gamma modulation during cueing in the object-based tracking group shares the same cortical sources with the tracking-related sustained gamma enhancement within the location-based tracking group. Both temporal morphologies emerge from the same principal component of the decomposition of the gamma signal including all subjects. Both group-specific morphologies load heavily on bilateral occipital sources, suggesting cortical processes to drive the observed gamma modulations rather than eye movements. The employed component analysis reliably identified such eye-movement artefacts within both observed gamma frequency ranges. The decomposition of the spectral signal has been established as the strategy to separate cognitive components and micro saccades during visual motion stimuli (Hipp & Siegel, 2013). For the current data, the corresponding factor loads concentrated heavily on frontal electrodes and sensors for the first components. Interestingly, the temporal morphology showed an elevated signal for this component mainly during the cueing period, which did not differ between groups. If at all, slight inter-group differences of those components during the tracking period entailed an opposite effect compared with the occipital gamma variation between groups of the cognitive source. This further strengthens the point that the increase in gamma signal during tracking within the location-based tracking group cannot be explained by microsaccadic variations. Furthermore, the independent component analysis used on the primary epoched data prior to subsequent analysis removed ocular spike potentials including micro saccades within the raw signal (Carl et al., 2012; Keren et al., 2010) in order to reduce ocular contamination of the electrophysiological signal even further. Additionally, measurements using an eye tracker in three control subjects confirmed that power modulations across the frequency spectrum were not elicited by micro saccades within posterior sites during the current tracking task. In sum, we are confident the observed modulations of gamma band activity are neither contaminated nor driven by micro saccades.

ACKNOWLEDGEMENT

This work was supported by the Deutsche Forschungsgemeinschaft Grant SFB1436/B05.

CONFLICT OF INTEREST

The authors have no conflicts of interest to declare.

AUTHOR CONTRIBUTIONS

C.M., J.-M.H. and M.A.S. conceived and designed the experiments. C.M. performed the experiments and conducted the analyses. C.M., J.-M.H. and M.A.S. interpreted the results of the experiments. C.M. prepared the figures and drafted the manuscript. C.M., J.-M.H. and M.A.S. edited and revised the manuscript and approved the final version of the manuscript.

PEER REVIEW

The peer review history for this article is available at https://publons.com/publon/10.1111/ejn.15605.

DATA AVAILABILITY STATEMENT

The data that support the findings of this study are available from the corresponding author upon reasonable request.

ORCID

Christian Merkel https://orcid.org/0000-0002-8730-5653

REFERENCES

Adjamian, P., Holliday, I. E., Barnes, G. R., Hillebrand, A., Hadjipapas, A., & Singh, K. D. (2004). Induced visual illusions and gamma oscillations in human primary visual cortex. *European Journal of Neuroscience*, *20*(2), 587–592. https://doi.org/10.1111/j.1460-9568.2004.03495.x

Alvarez, G. A., & Franconeri, S. L. (2007). How many objects can you track?: Evidence for a resource-limited attentive tracking mechanism. *Journal of Vision*, *7*(13), 14.1, 14–14.1410. https://doi.org/10.1167/7.13.14

Bastos, A. M., Vezoli, J., Bosman, C. A., Schoffelen, J.-M., Oostenveld, R., Dowdall, J. R., De Weerd, P., Kennedy, H., & Fries, P. (2015). Visual areas exert feedforward and feedback influences through distinct frequency channels. *Neuron*, *85*(2), 390–401. https://doi.org/10.1016/j.neuron.2014.12.018

Battaglini, L., Ghiani, A., Casco, C., & Ronconi, L. (2020). Parietal tACS at beta frequency improves vision in a crowding regime. *NeuroImage*, *208*, 116451. https://doi.org/10.1016/j.neuroimage.2019.116451

Belitski, A., Gretton, A., Magri, C., Murayama, Y., Montemurro, M. A., Logothetis, N. K., & Panzeri, S. (2008). Low-frequency local field potentials and spikes in primary visual cortex convey independent visual information. *Journal of Neuroscience*, *28*(22), 5696–5709. https://doi.org/10.1523/JNEUROSCI.0009-08.2008

Busch, N. A., & Herrmann, C. S. (2003). Object-load and feature-load modulate EEG in a short-term memory task. *Neuroreport*, *14*(13), 1721–1724. https://doi.org/10.1097/00001756-200309150-00013

Buschman, T. J., & Miller, E. K. (2007). Top-down versus bottom-up control of attention in the prefrontal and posterior parietal cortices. *Science*, *315*(5820), 1860–1862. https://doi.org/10.1126/science.1138071

Carl, C., Açık, A., König, P., Engel, A. K., & Hipp, J. F. (2012). The saccadic spike artifact in MEG. *NeuroImage*, *59*(2), 1657–1667. https://doi.org/10.1016/j.neuroimage.2011.09.020

Cavanagh, P., & Alvarez, G. (2005). Tracking multiple targets with multifocal attention. *Trends in Cognitive Sciences*, *9*(7), 349–354. https://doi.org/10.1016/j.tics.2005.05.009

Chen, W.-Y., Howe, P. D., & Holcombe, A. O. (2013). Resource demands of object tracking and differential allocation of the resource. *Attention, Perception, & Psychophysics*, *75*(4), 710–725. https://doi.org/10.3758/s13414-013-0425-1

Cowan, N. (2001). The magical number 4 in short-term memory: A reconsideration of mental storage capacity. *The Behavioral and Brain Sciences*, *24*(1), 87–114; discussion 114-185. https://doi.org/10.1017/s0140525x01003922

Donner, T. H., Siegel, M., Oostenveld, R., Fries, P., Bauer, M., & Engel, A. K. (2007). Population activity in the human dorsal pathway predicts the accuracy of visual motion detection. *Journal of Neurophysiology*, *98*(1), 345–359. https://doi.org/10.1152/jn.01141.2006

Drew, T., & Vogel, E. K. (2008). Neural measures of individual differences in selecting and tracking multiple moving objects. *Journal of Neuroscience*, *28*(16), 4183–4191. https://doi.org/10.1523/JNEUROSCI.0556-08.2008

Drisdelle, B. L., Aubin, S., & Jolicoeur, P. (2017). Dealing with ocular artifacts on lateralized ERPs in studies of visual-spatial attention and memory: ICA correction versus epoch rejection. *Psychophysiology*, *54*(1), 83–99. https://doi.org/10.1111/psyp.12675

Franconeri, S. L., Jonathan, S. V., & Scimeca, J. M. (2010). Tracking multiple objects is limited only by object spacing, not by speed, time, or capacity. *Psychological Science*, *21*(7), 920–925. https://doi.org/10.1177/0956797610373935

Fries, P. (2001). Modulation of oscillatory neuronal synchronization by selective visual attention. *Science*, *291*(5508), 1560–1563. https://doi.org/10.1126/science.1055465

Gevins, A., Smith, M. E., McEvoy, L., & Yu, D. (1997). High-resolution EEG mapping of cortical activation related to working memory: Effects of task difficulty, type of processing, and practice. *Cerebral Cortex*, *7*(4), 374–385. https://doi.org/10.1093/cercor/7.4.374

Gruber, T. (1999). Selective visual-spatial attention alters induced gamma band responses in the human EEG. *Clinical Neurophysiology*, *110*(12), 2074–2085. https://doi.org/10.1016/S1388-2457(99)00176-5

Hipp, J. F., Engel, A. K., & Siegel, M. (2011). Oscillatory synchronization in large-scale cortical networks predicts perception. *Neuron*, *69*(2), 387–396. https://doi.org/10.1016/j.neuron.2010.12.027

Hipp, J. F., & Siegel, M. (2013). Dissociating neuronal gamma-band activity from cranial and ocular muscle activity in EEG.

Frontiers in Human Neuroscience, *7*, 338. https://doi.org/10.3389/fnhum.2013.00338

Honkanen, R., Rouhinen, S., Wang, S. H., Palva, J. M., & Palva, S. (2015). Gamma oscillations underlie the maintenance of feature-specific information and the contents of visual working memory. *Cerebral Cortex*, *25*(10), 3788–3801. https://doi.org/10.1093/cercor/bhu263

Hoogenboom, N., Schoffelen, J.-M., Oostenveld, R., Parkes, L. M., & Fries, P. (2006). Localizing human visual gamma-band activity in frequency, time and space. *NeuroImage*, *29*(3), 764–773. https://doi.org/10.1016/j.neuroimage.2005.08.043

Howe, P. D., Horowitz, T. S., Morocz, I. A., Wolfe, J., & Livingstone, M. S. (2009). Using fMRI to distinguish components of the multiple object tracking task. *Journal of Vision*, *9*(4), 10.1, 10–10.1011. https://doi.org/10.1167/9.4.10

Iordanescu, L., Grabowecky, M., & Suzuki, S. (2009). Demand-based dynamic distribution of attention and monitoring of velocities during multiple-object tracking. *Journal of Vision*, *9*(4), 1.1, 1–1.112. https://doi.org/10.1167/9.4.1

Jensen, O., Gelfand, J., Kounios, J., & Lisman, J. E. (2002). Oscillations in the alpha band (9–12 Hz) increase with memory load during retention in a short-term memory task. *Cerebral Cortex*, *12*(8), 877–882. https://doi.org/10.1093/cercor/12.8.877

Jokisch, D., & Jensen, O. (2007). Modulation of gamma and alpha activity during a working memory task engaging the dorsal or ventral stream. *Journal of Neuroscience*, *27*(12), 3244–3251. https://doi.org/10.1523/JNEUROSCI.5399-06.2007

Jovicich, J., Peters, R. J., Koch, C., Braun, J., Chang, L., & Ernst, T. (2001). Brain areas specific for attentional load in a motion-tracking task. *Journal of Cognitive Neuroscience*, *13*(8), 1048–1058. https://doi.org/10.1162/089892901753294347

Kahneman, D., Treisman, A., & Gibbs, B. J. (1992). The reviewing of object files: Object-specific integration of information. *Cognitive Psychology*, *24*(2), 175–219. https://doi.org/10.1016/0010-0285(92)90007-O

Kaiser, J., Bühler, M., & Lutzenberger, W. (2004). Magnetoencephalographic gamma-band responses to illusory triangles in humans. *NeuroImage*, *23*(2), 551–560. https://doi.org/10.1016/j.neuroimage.2004.06.033

Kaiser, J., Ripper, B., Birbaumer, N., & Lutzenberger, W. (2003). Dynamics of gamma-band activity in human magnetoencephalogram during auditory pattern working memory. *NeuroImage*, *20*(2), 816–827. https://doi.org/10.1016/S1053-8119(03)00350-1

Kelly, S. P., Lalor, E. C., Reilly, R. B., & Foxe, J. J. (2006). Increases in alpha oscillatory power reflect an active retinotopic mechanism for distracter suppression during sustained visuospatial attention. *Journal of Neurophysiology*, *95*(6), 3844–3851. https://doi.org/10.1152/jn.01234.2005

Keren, A. S., Yuval-Greenberg, S., & Deouell, L. Y. (2010). Saccadic spike potentials in gamma-band EEG: Characterization, detection and suppression. *NeuroImage*, *49*(3), 2248–2263. https://doi.org/10.1016/j.neuroimage.2009.10.057

Kinsey, K., Anderson, S. J., Hadjipapas, A., & Holliday, I. E. (2011). The role of oscillatory brain activity in object processing and figure–ground segmentation in human vision. *International Journal of Psychophysiology*, *79*(3), 392–400. https://doi.org/10.1016/j.ijpsycho.2010.12.007

Klimesch, W., Sauseng, P., & Hanslmayr, S. (2007). EEG alpha oscillations: The inhibition–timing hypothesis. *Brain Research Reviews*, *53*(1), 63–88. https://doi.org/10.1016/j.brainresrev.2006.06.003

Kopell, N., Ermentrout, G. B., Whittington, M. A., & Traub, R. D. (2000). Gamma rhythms and beta rhythms have different synchronization properties. *Proceedings of the National Academy of Sciences*, *97*(4), 1867–1872. https://doi.org/10.1073/pnas.97.4.1867

Krause, C. M., Sillanmäki, L., Koivisto, M., Saarela, C., Häggqvist, A., Laine, M., & Hämäläinen, H. (2000). The effects of memory load on event-related EEG desynchronization and synchronization. *Clinical Neurophysiology*, *111*(11), 2071–2078. https://doi.org/10.1016/S1388-2457(00)00429-6

Lesch, H., Schoenfeld, M. A., & Merkel, C. (2020). Functional dissociation of multiple-object tracking mechanisms based on hemispheric asymmetries. *Restorative Neurology and Neuroscience*, *38*, 443–453. https://doi.org/10.3233/RNN-201048

Li, Y., Ma, Z., Lu, W., & Li, Y. (2006). Automatic removal of the eye blink artifact from EEG using an ICA-based template matching approach. *Physiological Measurement*, *27*(4), 425–436. https://doi.org/10.1088/0967-3334/27/4/008

Lutzenberger, W., Ripper, B., Busse, L., Birbaumer, N., & Kaiser, J. (2002). Dynamics of gamma-band activity during an audiospatial working memory task in humans. *Journal of Neuroscience*, *22*(13), 5630–5638. https://doi.org/10.1523/JNEUROSCI.22-13-05630.2002

McCusker, M. C., Wiesman, A. I., Schantell, M. D., Eastman, J. A., & Wilson, T. W. (2020). Multi-spectral oscillatory dynamics serving directed and divided attention. *NeuroImage*, *217*, 116927. https://doi.org/10.1016/j.neuroimage.2020.116927

Medendorp, W. P., Kramer, G. F. I., Jensen, O., Oostenveld, R., Schoffelen, J.-M., & Fries, P. (2007). Oscillatory activity in human parietal and occipital cortex shows hemispheric lateralization and memory effects in a delayed double-step saccade task. *Cerebral Cortex*, *17*(10), 2364–2374. https://doi.org/10.1093/cercor/bhl145

Merkel, C., Hopf, J.-M., Heinze, H.-J., & Schoenfeld, M. A. (2015). Neural correlates of multiple object tracking strategies. *NeuroImage*, *118*, 63–73. https://doi.org/10.1016/j.neuroimage.2015.06.005

Merkel, C., Hopf, J.-M., & Schoenfeld, M. A. (2017). Spatio-temporal dynamics of attentional selection stages during multiple object tracking. *NeuroImage*, *146*, 484–491. https://doi.org/10.1016/j.neuroimage.2016.10.046

Merkel, C., Hopf, J.-M., & Schoenfeld, M. A. (2020). How to perceive object permanence in our visual environment: The multiple object tracking paradigm. In S. Pollmann (Ed.), *Spatial learning and attention guidance* (pp. 157–176). Springer US. https://doi.org/10.1007/7657_2019_28

Merkel, C., Stoppel, C. M., Hillyard, S. A., Heinze, H.-J., Hopf, J.-M., & Schoenfeld, M. A. (2014). Spatio-temporal patterns of brain activity distinguish strategies of multiple-object tracking. *Journal of Cognitive Neuroscience*, *26*(1), 28–40. https://doi.org/10.1162/jocn_a_00455

Michalareas, G., Vezoli, J., van Pelt, S., Schoffelen, J.-M., Kennedy, H., & Fries, P. (2016). Alpha-beta and gamma rhythms subserve feedback and feedforward influences among

human visual cortical areas. *Neuron*, *89*(2), 384–397. https://doi.org/10.1016/j.neuron.2015.12.018

Morgan, H. M., Muthukumaraswamy, S. D., Hibbs, C. S., Shapiro, K. L., Bracewell, R. M., Singh, K. D., & Linden, D. E. J. (2011). Feature integration in visual working memory: Parietal gamma activity is related to cognitive coordination. *Journal of Neurophysiology*, *106*(6), 3185–3194. https://doi.org/10.1152/jn.00246.2011

Okada, Y. C., & Salenius, S. (1998). Roles of attention, memory, and motor preparation in modulating human brain activity in a spatial working memory task. *Cerebral Cortex*, *8*(1), 80–96. https://doi.org/10.1093/cercor/8.1.80

Okazaki, M., Kaneko, Y., Yumoto, M., & Arima, K. (2008). Perceptual change in response to a bistable picture increases neuromagnetic beta-band activities. *Neuroscience Research*, *61*(3), 319–328. https://doi.org/10.1016/j.neures.2008.03.010

Oostenveld, R., Fries, P., Maris, E., & Schoffelen, J.-M. (2011). FieldTrip: Open source software for advanced analysis of MEG, EEG, and invasive electrophysiological data. *Computational Intelligence and Neuroscience*, *2011*, 1–9. https://doi.org/10.1155/2011/156869

Palva, S., Kulashekhar, S., Hamalainen, M., & Palva, J. M. (2011). Localization of cortical phase and amplitude dynamics during visual working memory encoding and retention. *Journal of Neuroscience*, *31*(13), 5013–5025. https://doi.org/10.1523/JNEUROSCI.5592-10.2011

Pesonen, M., Hämäläinen, H., & Krause, C. M. (2007). Brain oscillatory 4–30 Hz responses during a visual n-back memory task with varying memory load. *Brain Research*, *1138*, 171–177. https://doi.org/10.1016/j.brainres.2006.12.076

Pfurtscheller, G. (2001). Functional brain imaging based on ERD/-ERS. *Vision Research*, *41*(10), 1257–1260. https://doi.org/10.1016/S0042-6989(00)00235-2

Pylyshyn, Z. (1989). The role of location indexes in spatial perception: A sketch of the FINST spatial-index model. *Cognition*, *32*(1), 65–97. https://doi.org/10.1016/0010-0277(89)90014-0

Pylyshyn, Z. (2004). Some puzzling findings in multiple object tracking: I. Tracking without keeping track of object identities. *Visual Cognition*, *11*(7), 801–822. https://doi.org/10.1080/13506280344000518

Richter, C. G., Thompson, W. H., Bosman, C. A., & Fries, P. (2017). Top-down beta enhances bottom-up gamma. *The Journal of Neuroscience*, *37*(28), 6698–6711. https://doi.org/10.1523/JNEUROSCI.3771-16.2017

Ronconi, L., Bertoni, S., & Bellacosa Marotti, R. (2016). The neural origins of visual crowding as revealed by event-related potentials and oscillatory dynamics. *Cortex*, *79*, 87–98. https://doi.org/10.1016/j.cortex.2016.03.005

Rouhinen, S., Panula, J., Palva, J. M., & Palva, S. (2013). Load dependence of β and γ oscillations predicts individual capacity of visual attention. *Journal of Neuroscience*, *33*(48), 19023–19033. https://doi.org/10.1523/JNEUROSCI.1666-13.2013

Sauseng, P., Klimesch, W., Doppelmayr, M., Pecherstorfer, T., Freunberger, R., & Hanslmayr, S. (2005). EEG alpha synchronization and functional coupling during top-down processing in a working memory task. *Human Brain Mapping*, *26*(2), 148–155. https://doi.org/10.1002/hbm.20150

Sauseng, P., Klimesch, W., Heise, K. F., Gruber, W. R., Holz, E., Karim, A. A., Glennon, M., Gerloff, C., Birbaumer, N., & Hummel, F. C. (2009). Brain oscillatory substrates of visual short-term memory capacity. *Current Biology*, *19*(21), 1846–1852. https://doi.org/10.1016/j.cub.2009.08.062

Scholl, B. J., Pylyshyn, Z. W., & Feldman, J. (2001). What is a visual object? Evidence from target merging in multiple object tracking. *Cognition*, *80*(1–2), 159–177. https://doi.org/10.1016/S0010-0277(00)00157-8

Shim, W. M., Alvarez, G. A., & Jiang, Y. V. (2008). Spatial separation between targets constrains maintenance of attention on multiple objects. *Psychonomic Bulletin & Review*, *15*(2), 390–397. https://doi.org/10.3758/PBR.15.2.390

Siegel, M., Donner, T. H., Oostenveld, R., Fries, P., & Engel, A. K. (2007). High-frequency activity in human visual cortex is modulated by visual motion strength. *Cerebral Cortex*, *17*(3), 732–741. https://doi.org/10.1093/cercor/bhk025

Singh, K. D., Barnes, G. R., Hillebrand, A., Forde, E. M. E., & Williams, A. L. (2002). Task-related changes in cortical synchronization are spatially coincident with the hemodynamic response. *NeuroImage*, *16*(1), 103–114. https://doi.org/10.1006/nimg.2001.1050

Tallon-Baudry, C., Bertrand, O., Hénaff, M.-A., Isnard, J., & Fischer, C. (2005). Attention modulates gamma-band oscillations differently in the human lateral occipital cortex and fusiform gyrus. *Cerebral Cortex*, *15*(5), 654–662. https://doi.org/10.1093/cercor/bhh167

Tallon-Baudry, C., Bertrand, O., Peronnet, F., & Pernier, J. (1998). Induced γ-band activity during the delay of a visual short-term memory task in humans. *Journal of Neuroscience*, *18*(11), 4244–4254. https://doi.org/10.1523/JNEUROSCI.18-11-04244.1998

Tallon-Baudry, C., Bertrand, O., Wienbruch, C., Ross, B., & Pantev, C. (1997). Combined EEG and MEG recordings of visual 40 Hz responses to illusory triangles in human. *Neuroreport*, *8*(5), 1103–1107. https://doi.org/10.1097/00001756-199703240-00008

Vidal, J. R., Chaumon, M., O'Regan, J. K., & Tallon-Baudry, C. (2006). Visual grouping and the focusing of attention induce gamma-band oscillations at different frequencies in human magnetoencephalogram signals. *Journal of Cognitive Neuroscience*, *18*(11), 1850–1862. https://doi.org/10.1162/jocn.2006.18.11.1850

von Stein, A., Chiang, C., & Konig, P. (2000). Top-down processing mediated by interareal synchronization. *Proceedings of the National Academy of Sciences*, *97*(26), 14748–14753. https://doi.org/10.1073/pnas.97.26.14748

Worden, M. S., Foxe, J. J., Wang, N., & Simpson, G. V. (2000). Anticipatory biasing of visuospatial attention indexed by retinotopically specific α-bank electroencephalography increases over occipital cortex. *Journal of Neuroscience*, *20*(6), RC63–RC63. https://doi.org/10.1523/JNEUROSCI.20-06-j0002.2000

Wutz, A., Zazio, A., & Weisz, N. (2020). Oscillatory bursts in parietal cortex reflect dynamic attention between multiple objects and ensembles. *The Journal of Neuroscience*, *40*, 6927, JN-RM-0231-20–6937. https://doi.org/10.1523/JNEUROSCI.0231-20.2020

Yantis, S. (1992). Multielement visual tracking: Attention and perceptual organization. *Cognitive Psychology*, *24*(3), 295–340. https://doi.org/10.1016/0010-0285(92)90010-Y

Zaretskaya, N., & Bartels, A. (2015). Gestalt perception is associated with reduced parietal beta oscillations. *NeuroImage*, *112*, 61–69. https://doi.org/10.1016/j.neuroimage.2015.02.049

SUPPORTING INFORMATION

Additional supporting information may be found in the online version of the article at the publisher's website.

How to cite this article: Merkel, C., Hopf, J.-M., & Schoenfeld, M. A. (2022). Electrophysiological hallmarks of location-based and object-based visual multiple objects tracking. *European Journal of Neuroscience*, *55*(5), 1200–1214. https://doi.org/10.1111/ejn.15605